

Access of solar wind electrons into the Martian magnetosphere

E. M. Dubinin¹, M. Fraenz¹, J. Woch¹, E. Roussos¹, J. D. Winningham², R. A. Frahm², A. Coates³, F. Leblanc⁴, R. Lundin⁵, and S. Barabash⁵

¹Max-Planck-Institute für Sonnensystemforschung, Lindau, Germany

²Southwest Research Institute, San-Antonio, USA

³MSSL, University College London, UK

⁴Observatorio Astronomico di Trieste, Trieste, Italy

⁵Swedish Institute of Space Physics, Kiruna, Sweden

Received: 10 January 2008 – Revised: 9 October 2008 – Accepted: 15 October 2008 – Published: 12 November 2008

Abstract. Electrons with energy of $\sim 40\text{--}80$ eV measured by the instrument ASPERA-3 on Mars Express and MAG-ER onboard Mars Global Surveyor are used to trace an access of solar wind electrons into the Martian magnetosphere. Crustal magnetic fields create an additional protection from solar wind plasma on the dayside of the Southern Hemisphere by shifting the boundary of the induced magnetosphere (this boundary is often referred as the magnetic pileup boundary) above strong crustal sources to ~ 400 km as compared to the Northern Hemisphere. Localized intrusions through cusps are also observed. On the nightside an access into the magnetosphere depends on the IMF orientation. Negative values of the $B_{y\text{IMF}}$ component assist the access to the regions with strong crustal magnetizations although electron fluxes are strongly weakened below ~ 600 km. A precipitation pattern at lower altitudes is formed by intermittent regions with reduced and enhanced electron fluxes. The precipitation sites are longitudinally stretched narrow bands in the regions with a strong vertical component of the crustal field. Fluxes $\geq 10^9$ cm⁻² s⁻¹ of suprathermal electrons necessary to explain the observed aurora emissions are maintained only for the periods with enhanced precipitation. The appearance of another class of electron distributions – inverted V structures, characterized by peaks on energy spectra, is controlled by the IMF. They are clustered in the hemisphere pointed by the interplanetary electric field that implies a constraint on their origin.

Keywords. Magnetospheric physics (Magnetopause, cusp, and boundary layers; Planetary magnetospheres; Solar wind interactions with unmagnetized bodies)

Correspondence to: E. M. Dubinin
(dubinin@mps.mpg.de)

1 Introduction

Mars presents a nonmagnetized, conducting (due to the presence of the ionosphere) obstacle to solar wind with local magnetizations. As a result, a picture of interaction arises that is rather complicated and variable – with main elements of induced and some of intrinsic magnetospheres. Electron measurements provide us with an effective tool to monitor the plasma morphology and processes within the Martian magnetosphere. For example, the observations of solar halo electrons in the Martian tail on Phobos-2 revealed signatures which were interpreted as indication of a putative planetary magnetic field (Dubinin et al., 1994). Note that the direct measurements of the magnetic field near the planet by Mars Global Surveyor have shown that presently Mars has no a global magnetic field. Instead, MGS has detected localized, rather strong magnetic anomalies of a crustal origin (Acuña et al., 1998). It was shown that the crustal magnetic fields act as an additional screen protecting the lower atmosphere/ionosphere from direct contact with solar wind (Fraenz et al., 2006). On the other hand, narrow channels for electron penetration, similar to the Earth's cusps were also found from the electron measurements (Soobiah et al., 2006). The extent and variability of the Martian ionosphere was investigated by Mitchell et al. (2001) using the electron observations on Mars Global Surveyor. Analyzing the shape of electron pitch-angle distributions Brain et al. (2007) have inferred a topology of magnetic field lines. Brain et al. (2007) could distinguish between closed, open and draped field lines. Mitchell et al. (2007) inferred a magnetic field pattern below 400 km altitude with implications for the formation mechanisms of the dichotomy on Mars from analysis of electron angular distributions. Analysis of electron data in a time-frequency domain showed the existence of rather coherent oscillations in the magnetosheath and magnetospheric

plasmas (Winningham et al., 2006). Observations of peaked electron distributions on Mars Global Surveyor and Mars Express which are similar to the inverted V structures related to the aurora on Earth (Brain et al., 2006a; Lundin et al., 2006) raised the very interesting question whether aurora exists on Mars. The observations of energy peaks in the range of 20–30 eV on electron spectra related to CO₂-photoelectrons allows tracing of ionospheric plasma far from Mars (Dubinin et al., 2006; Frahm et al., 2006) which is important for our understanding of mechanisms of ion scavenging. Here we present further observations made by the electron spectrometer ELS on Mars Express (MEX) to infer a picture of access of solar wind electrons into the Martian magnetosphere based on more than two years of ASPERA-3 measurements. In some cases the data are complemented by the measurements made on Mars Global Surveyor (MGS).

The layout of the paper is as follows. Section 2 contains the description of the instrumentation. Section 3 contains the results of observations. Section 3.1 discusses the role of crustal fields on the position of the magnetospheric boundary on the dayside and access of solar wind electrons into the magnetosphere. It is shown that strong crustal sources in the Southern Hemisphere shift upward the magnetospheric boundary producing a distinct asymmetry. The crustal magnetizations operate mainly as an additional screen to solar wind although examples of plasma intrusions through the mini cusps are also found. Sections 3.2 and 3.3 consider a problem of electron access on the nightside. An important role of the external factors (the IMF orientation) is found. It is shown that efficient screening of crustal magnetic fields extends up to ~600 km. Asymmetry in electron access due to the Parker shape of the IMF is also observed. The next Sect. 3.4, discusses precipitation patterns of electrons at lower altitudes (≤ 400 km) and their relationship with aurora on Mars. Last subsection analyze a spatial distribution of the events with peaked electron spectra which were considered as another potential candidate for aurora on Mars. A mechanism of the generation of such electron distribution is also discussed.

2 Instrumentation

The ELS instrument is a spherical top hat analyzer and is a part of the ASPERA-3 experiment (Barabash et al., 2006). It measures 2-D distributions of electron fluxes in the energy range 1 eV–20 keV (the grid is usually biased at -5 V and protects from the low energy ionospheric electrons) with energy resolution of $\delta E/E \sim 8\%$, a field of view of $4^\circ \times 360^\circ$ divided into 16 sectors, and a time resolution of ~ 4 s per energy spectrum (128 energy steps). More details about the instrument can be found in Barabash et al. (2006).

The Electron Reflectometer (ER) is a part of the MGS-ER experiment onboard MGS (Acuña et al., 1992). It also consists of a hemispherical electrostatic analyzer followed

by a microchannel plate and anode divided on 16 sectors. Field of view and energy resolution of ER are, respectively, $14^\circ \times 360^\circ$ and 20%. The measurements are made in the range 1 eV–20 keV (30 energy steps). A more complete description can be found in Mitchell et al. (2001).

Here we use observations made in the energy range 40–80 eV (ELS) and 30–80 eV (ER) from 2004 through April 2006 (in some cases the analysis was extended through March 2007). These energies are typical for magnetosheath electrons and can be used to trace an access of solar wind electrons into the Martian magnetosphere (see e.g. Dubinin et al., 2006; Fraenz et al., 2006). The data from both spacecraft will be presented in the units of total flux F in this energy range where $F=4\pi J \Delta E$. Here J is a differential flux ($\text{cm}^{-2} \text{s}^{-1} \text{ster}^{-1} \text{eV}^{-1}$) averaged over all 16 azimuth directions, $\Delta E=40$ eV and we assume an isotropic electron flux.

3 Observations

3.1 Access of solar wind electrons on the dayside

The boundary determined from a drop of fluxes of the magnetosheath electrons which coincides with a boundary of a “stoppage” of the solar wind is an induced magnetospheric boundary (MB) formed by the solar wind interaction with the Martian ionosphere and upper atmosphere (Dubinin et al., 2006, and references therein). The boundary has been often referred as the magnetic pileup boundary (Bertucci et al., 2003; Nagy et al., 2004). Crustal magnetic fields can contribute to the total pressure of the obstacle against the solar wind (Crider et al., 2002; Dubinin et al., 2006). Figure 1 shows maps of total electron fluxes ($40 \text{ eV} < E_e < 80 \text{ eV}$) on the dayside in cylindrical coordinates. A bin size is $0.03 R_M \times 0.03 R_M$. The maps show the median values of fluxes in a bin. The data are given for the Northern and Southern Hemispheres but only for planetocentric longitudes $130^\circ < \text{Long} < 240^\circ$. Note that the strongest crustal magnetizations on Mars are located in this sector of the Southern Hemisphere. Black and red shaded bins have fluxes higher (less) than the maximum (minimum) value in the color bar. Average positions of the bow shock (BS) and the magnetospheric boundary (MB) determined, respectively, from the MGS and MEX observations (Vignes et al., 2000; Dubinin et al., 2006) are also shown. It is worth noting that the model of the MB position based both on MGS and Phobos-2 observations (Trotignon et al., 2006) gives a reasonable agreement with the above mentioned models. It is seen that the MB moves upward in the Southern Hemisphere (dashed curve) that is in the agreement with the MGS observations (Crider et al., 2002). At solar zenith angles $\text{SZA} \geq 45^\circ$ the shift reaches ~ 500 km. In fact, the boundary may have not a smooth but a corrugated shape due to a local and not uniform origin of crustal magnetization. Such examples were presented by Dubinin et al. (2008a). It is also worth noting that a shift of the

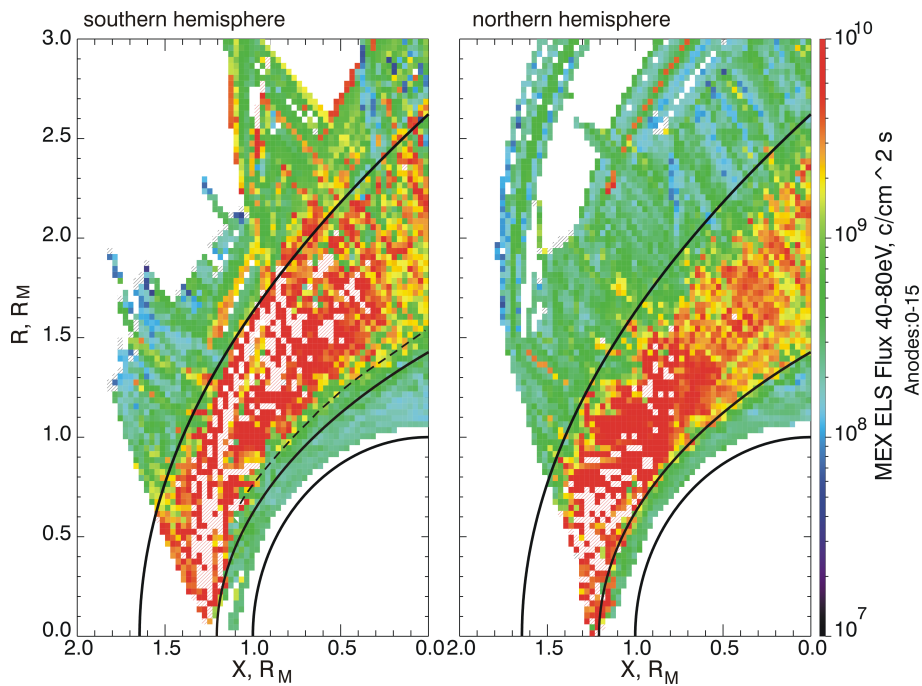


Fig. 1. Maps of total median electron fluxes ($40\text{ eV} < E < 80\text{ eV}$) on the dayside for the Northern and Southern Hemispheres at the range of longitudes $130^\circ < \text{Long} < 240^\circ$. Solid curves show statistical average positions of the magnetospheric boundary (MB) (Dubinin et al., 2006) and the bow shock (BS) (Vignes et al., 2000). Dashed curve gives a shift of the MB above the crustal magnetic sources.

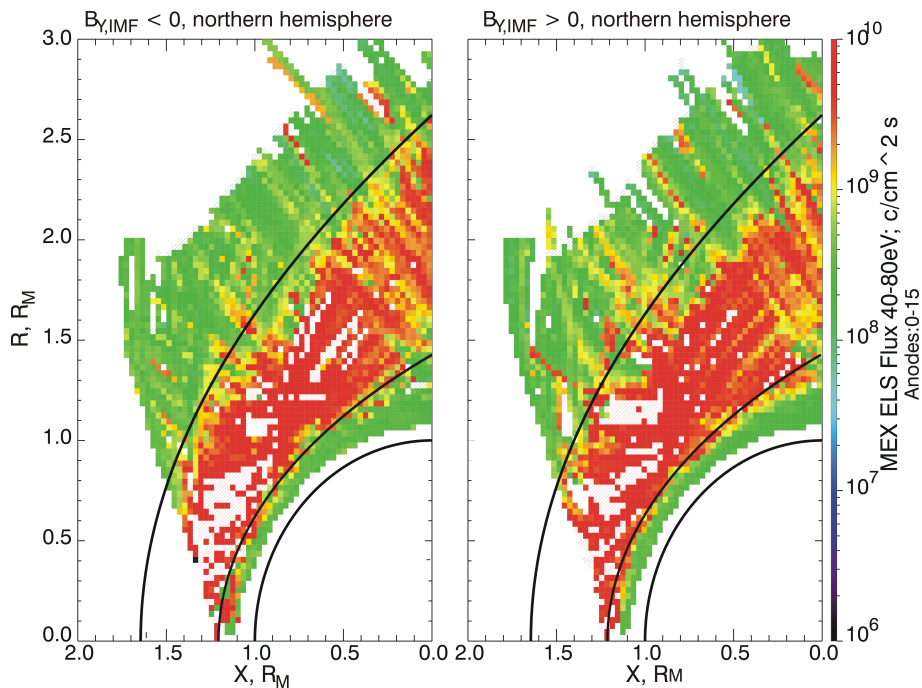


Fig. 2. Maps of electron fluxes in the Northern dayside Hemisphere for $B_{y,IMF} < 0$, and $B_{y,IMF} > 0$.

magnetospheric boundary influences the position of the bow shock. It goes further from the planet above the region of strong crustal magnetization. This effect was not observed

in the previous study based on the MGS and MEX observations without constraints on the longitude range (Vignes et al., 2002; Dubinin et al., 2008a).

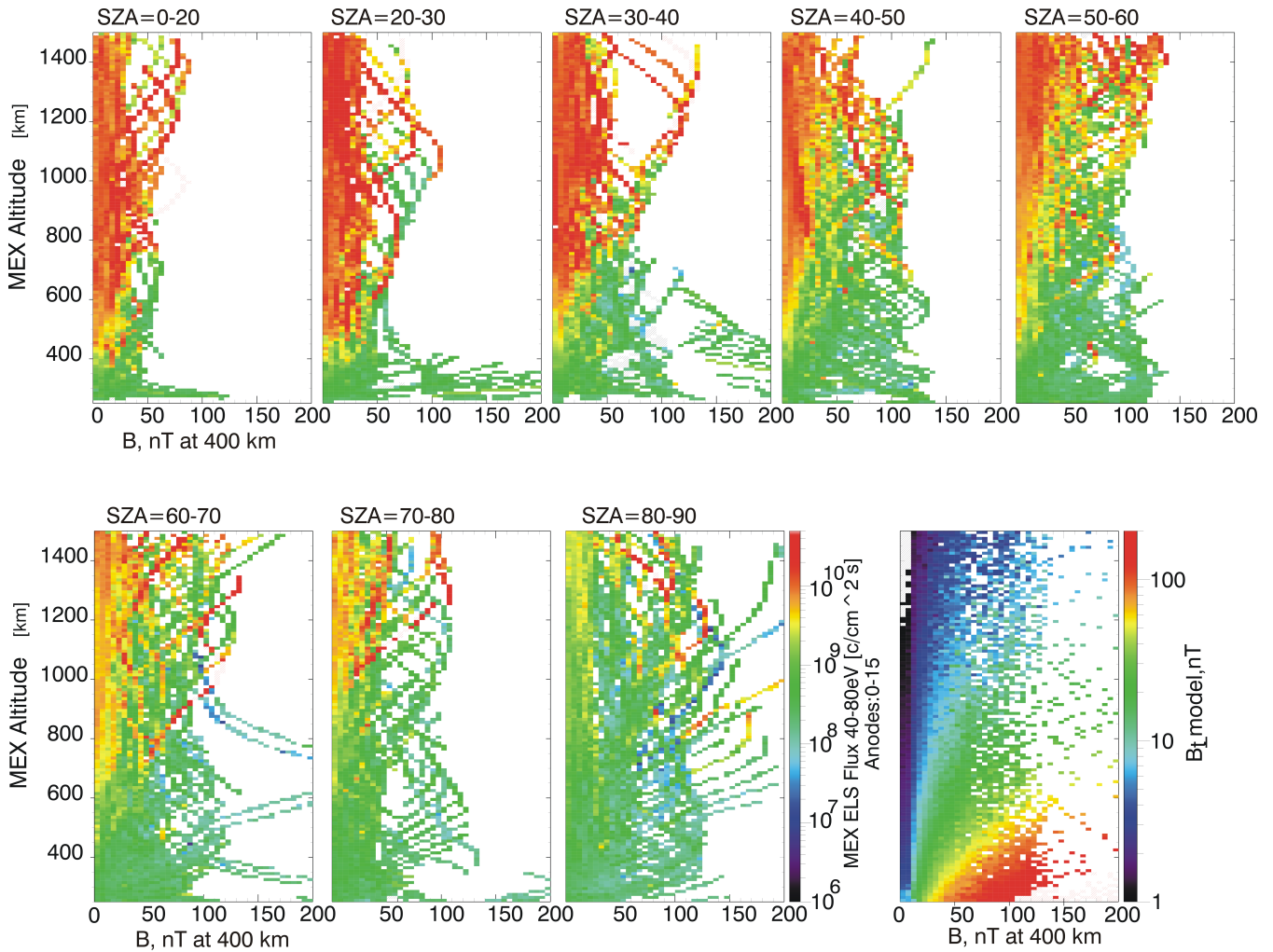


Fig. 3. Maps of electron access as a function of the strength of the crustal field B_{cr} at the altitude of 400 km and altitude (h) of the spacecraft for different solar zenith angles. (right panel) crustal magnetic field strength inferred from the model by Cain et al. (2003).

Vennerstrom et al. (2003) have shown that piled up magnetic field is stronger in the hemisphere into which the motional electric field is pointing. A similar effect was observed in hybrid simulations of the solar wind interaction with Mars (Böswetter et al., 2004; Modolo et al., 2005). Figure 2 shows maps of electron fluxes for the Northern dayside Hemisphere (where effects of crustal fields are small) for different signs of the B_y component of the IMF. A proxy direction of the $B_{y,IMF}$ component was inferred from the MGS observations assuming that the magnetic field at middle latitudes of the Northern Hemisphere is primarily of induced origin (Brain et al., 2006b; Dubinin et al., 2006; Fedorov et al., 2006). A positive sign corresponds to the case when piled up magnetic field is expected to be higher in the Northern Hemisphere. However, we do not observe visible signatures of asymmetry in the MB positions. More careful analysis based on real magnetic field observations, instead of a proxy method, is required to clarify this feature.

Using the ASPERA-3 data Fraenz et al. (2006) have shown that on the dayside the altitude of electron access decreases almost linearly with increase of the strength of crustal magnetizations. Fraenz et al. (2006) have made an average over the whole range of solar zenith angles on the dayside. Here, using better statistics, we present the data for a set of different zenith angles to infer an effect of the strength of crustal field more accurately. The panels in Fig. 3 show maps of electron access as a function of the strength of the crustal field B at the altitude of 400 km and altitude (h) for different solar zenith angles. An upward, approximately linear shift of the “access boundary” with increase of the magnetic field strength is observed at solar zenith angles $SZA \geq 30^\circ$ on the dayside. Such a dependence is clearly revealed, for example, at $SZA \sim 30\text{--}60^\circ$ at which the data coverage is higher.

The right panel shows in the same format the values of the crustal magnetic field from multiple sources according to the model by Cain et al. (2003). The magnetic

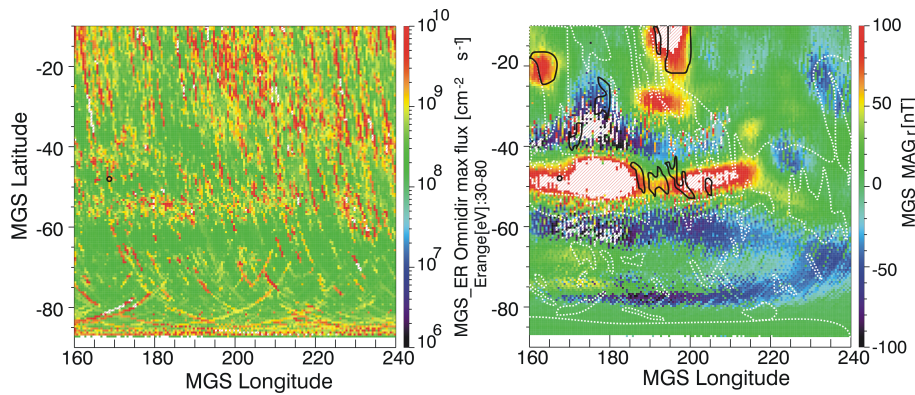


Fig. 4. (a) Precipitation pattern of electrons at 400 km from the MGS observations; (b) Map of the vertical component B_r of the crustal field based on the results by Connerney et al. (2001). Regions of enhanced precipitation are bounded by dotted white curves and solid black curves. A black circle at $\text{Lat}=-48^\circ$, $\text{Long}=167.5^\circ$ corresponds to the foot of cusp detected on 7 July 2007.

field strength at the altitude of the boundary is about 15–20 nT. The interesting question is whether the magnetic field of the crustal sources is able to balance the solar wind pressure. In the kinetic approximation the pressure exerted by the magnetosheath plasma at the magnetopause, $p \approx K \rho V^2 \cos^2(\text{SZA})$, where ρV^2 is the dynamic solar wind pressure ($\rho = n_p m_p$, n_m and m_p are the proton number density and mass, respectively), and the factor $K=0.88$. For the mean solar wind conditions at the orbit of Mars, $n_p \sim 2 \text{ cm}^{-3}$, $V \sim 500 \text{ km/s}$ and $\text{SZA} \sim 45^\circ$, a pressure balance yields $B = (8\pi K \rho V^2 \cos^2(\text{SZA}))^{1/2} \sim 30 \text{ nT}$. The corresponding “vacuum” magnetic field without a contribution due to the Chapman-Ferraro currents on the magnetopause is about 15–20 nT that is in a reasonable agreement with the magnetic field value of crustal sources. However, it is not clear yet whether the Earth-type magnetopause can be formed above the local regions with strong crustal magnetizations or both factors, a pile-up of the interplanetary magnetic field and compression of the crustal magnetic field, provide us with a larger scale to the magnetospheric obstacle.

A comparison of the map of electron fluxes on the day side in the planetocentric longitude-latitude coordinates with the map of the crustal field based on the MGS observations at the altitude of 400 km is shown in Fig. 4. A “precipitation” pattern of solar electrons in the region of strong crustal fields is rather irregular but some trends are visible. Regions of enhanced precipitation are bounded by white dotted curves and imposed on the magnetic field map (the right panel). Penetrating electrons are measured mainly in the areas with small values of the vertical component (colored green) that is in accordance with observations by Fraenz et al. (2006) and the results presented in the previous section. However there are also clear signatures of cusp-like features (some of them are bounded by black solid curves). Maximum values of electron fluxes often reach $\sim 10^{10} \text{ cm}^{-2} \text{ s}^{-1}$ and therefore can easily produce optical emissions in the lower altitude atmosphere.

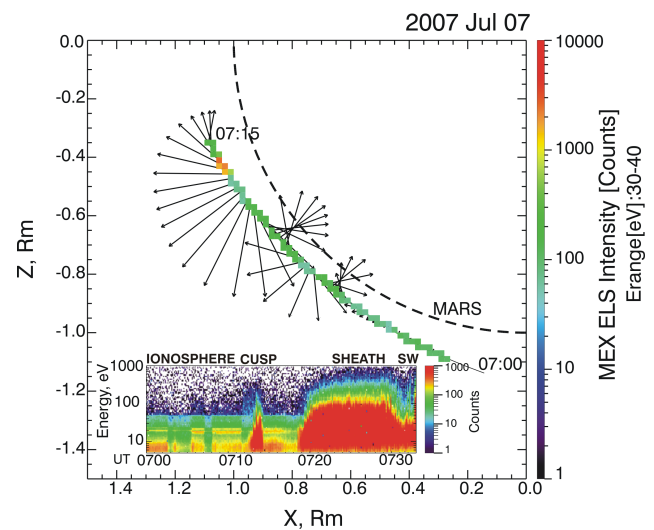


Fig. 5. Vectors of crustal field in the XZ-MSO plane along the MEX trajectory. Color bars along the orbit show electron flux (counts) in the energy range 30–40 eV. A red spot corresponds to the cusp crossing. Energy-time spectrogram of electron fluxes that shows the main plasma domains (ionosphere, cusp, sheath and solar wind) is inserted.

An energy-time spectrogram of electron fluxes measured along the MEX trajectory on 7 July 2007 (Fig. 5) depicts an example of a cusp signature. At $\sim 07:13$ the spacecraft, moving within the ionosphere, that is clearly recognized from the observations of two spectral peaks of CO_2 photoelectrons (20–30 eV), records an intense spike of magnetosheath-like electrons ($h \sim 430 \text{ km}$, $\text{SZA} \sim 22^\circ$). Then MEX subsequently reenters the ionosphere and enters the magnetosheath and solar wind at 07:14, 07:19 and 07:31, respectively. A projection of the MEX trajectory onto the XZ MSO plane with the vectors of the crustal field along the orbit inferred from the Cain’ model is also shown in Fig. 5. Color bars along

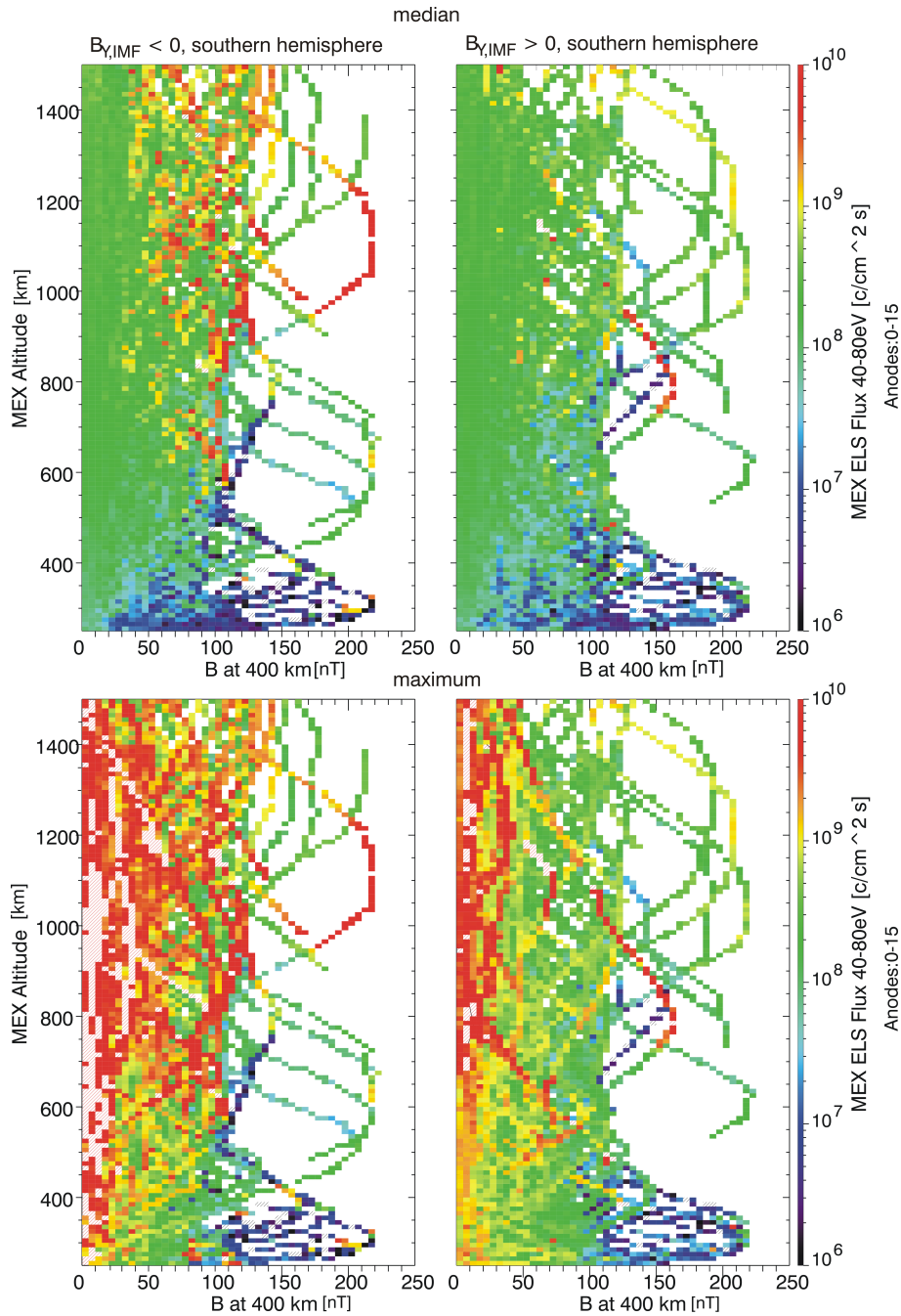


Fig. 6. Total median (top panels) and maximum (bottom panels) fluxes of electrons ($40 \text{ eV} < E_e < 80 \text{ eV}$) on the nightside of the Southern Hemisphere as a function of the crustal field strength and altitude for $B_{y,IMF} > 0$ and $B_{y,IMF} < 0$.

the trajectory present the electron fluxes ($E_e = 30\text{--}40 \text{ eV}$) measured by ASPERA-ELS. Crossing of the cusp characterized by the appearance of intruding sheath-like electrons occurs in the region with strong crustal field. A position of the cusp signature in the planetocentric latitude-longitude coordinates (Fig. 4) is shown by the circle (Long= 167.5° , Lat= -48°).

3.2 Access of solar wind electrons on the nightside

To study the shielding efficiency of crustal magnetic fields on the nightside we plot the total flux ($\text{cm}^{-2} \text{ s}^{-1}$) of electrons with $40 \text{ eV} < E_e < 80 \text{ eV}$ in the Southern Hemisphere as a function of the magnetic field strength B_{cr} at 400 km (Connerney et al., 2001) and the altitude h . Here again the data were sorted by the sign of the B_y component of the IMF

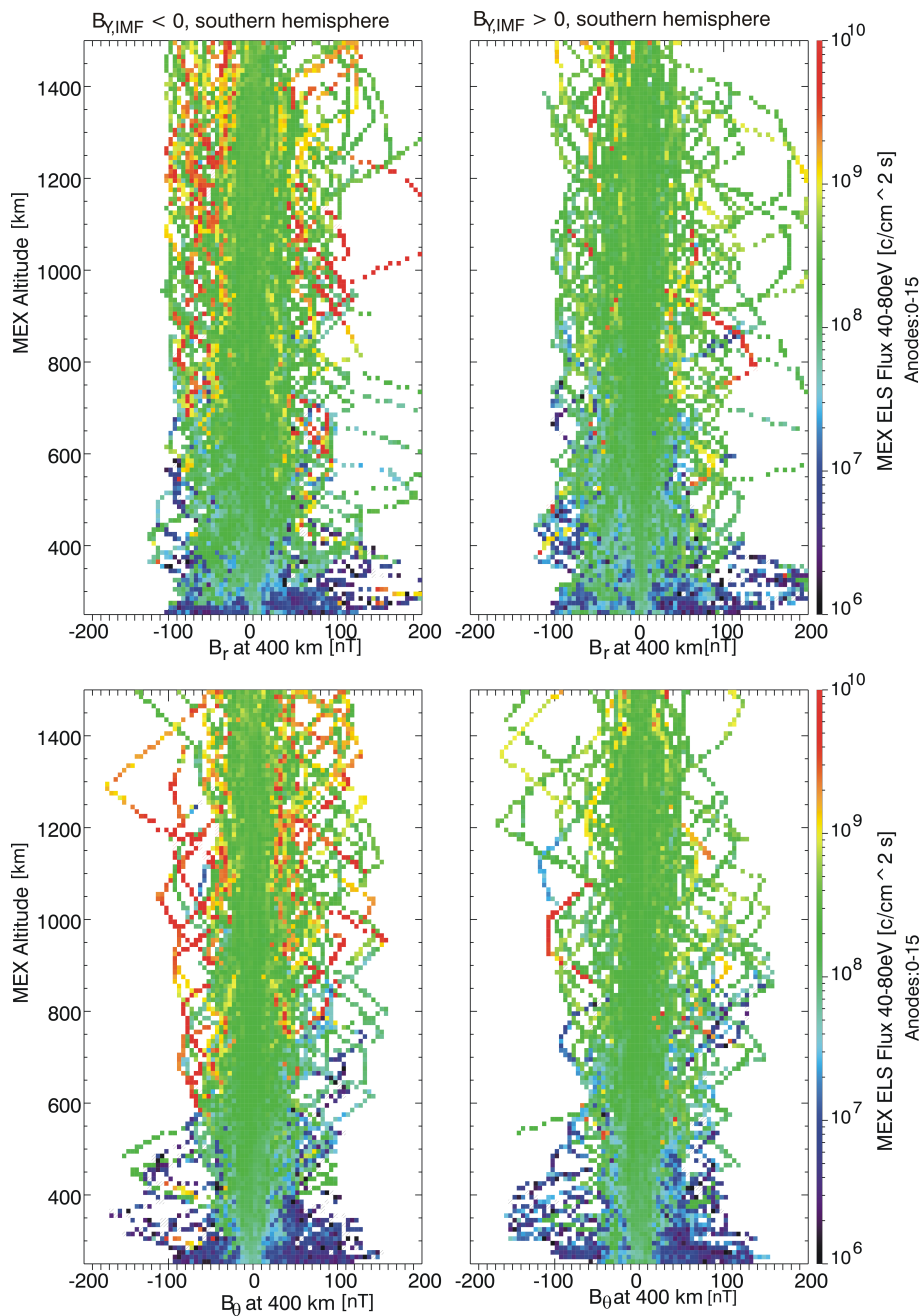


Fig. 7. Total median flux of electrons ($40\text{ eV} < E_e < 80\text{ eV}$) on the nightside of the Southern Hemisphere as a function of the vertical (B_r) and horizontal (B_θ) and altitude for $B_{y,IMF} > 0$ and $B_{y,IMF} < 0$.

(Fig. 6). The bin size is $5\text{ nT} \times 10\text{ km}$. The upper (lower) pair of panels shows the data with the median (maximum) values of fluxes in a bin. At the “median” conditions, electrons with fluxes of about $10^8\text{ cm}^{-2}\text{ s}^{-1}$ have easy access to low altitudes only in the regions with small crustal fields. Crustal fields with a strength $> 50\text{ nT}$ rather effectively screen the low altitude atmosphere although localized intrusions are observed at $h \sim 300\text{ km}$. Note here that typical electron fluxes at altitudes $300\text{--}400\text{ km}$ are less than $10^7\text{ cm}^{-2}\text{ s}^{-1}$.

A strong asymmetry caused by the IMF orientation is clearly seen (see also Roussos et al., 2007). For the IMF with $B_y < 0$ electrons with fluxes of about $10^8\text{ cm}^{-2}\text{ s}^{-1}$ are observed at the altitudes $\geq 600\text{ km}$ above strong crustal sources. Their absence above the planetary regions with a weak crustal field indicates that crustal fields for a favorable IMF orientation allow an access of solar wind electrons, at least, to the altitudes $\sim 600\text{ km}$. A more easy access could be due to reconnection between the draped magnetic field of

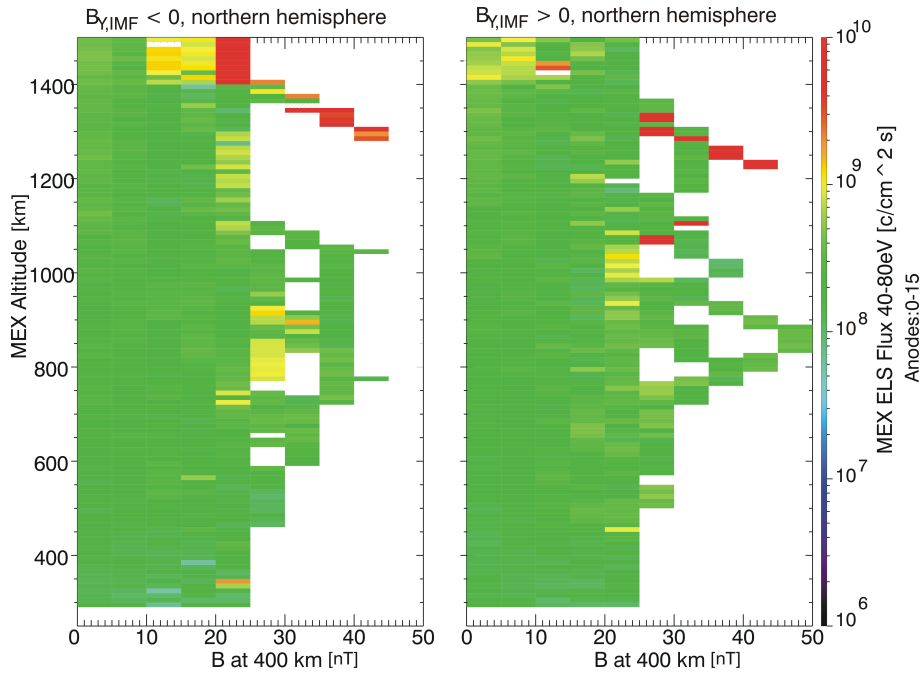


Fig. 8. Total median flux of electrons ($40 \text{ eV} < E_e < 80 \text{ eV}$) on the nightside of the Northern Hemisphere as a function of the crustal field strength and altitude for $B_{y,IMF} > 0$ and $B_{y,IMF} < 0$.

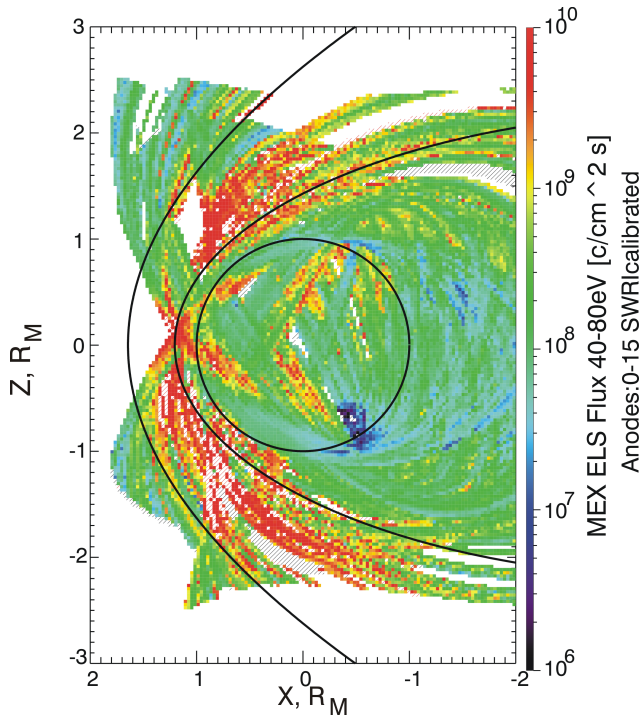


Fig. 9. Map of median electron fluxes ($40 \text{ eV} < E < 80 \text{ eV}$) in the XZ (MSO) noon-midnight plane.

solar wind and crustal fields. Multiple current sheets arising in different reconnection sites are also the additional sources for enhanced electron fluxes. The control by the sign of $B_{y,IMF}$ probably implies that draped magnetic fields of the solar wind origin penetrate inward more efficiently in the hemisphere into which the motional electric field is pointing. A joint effect of these factors can produce the observed asymmetry.

A magnetic shielding at $B_{cr} \geq 100 \text{ nT}$ exists even for “extreme” conditions which are shown in the lower panels and depict maximum values of electron fluxes in the bins. For $B_y > 0$ the intensity of electron fluxes decreases with altitude ($< 600 \text{ km}$) even if $B_{cr} < 20\text{--}30 \text{ nT}$. The intensity of the electron fluxes significantly increases for the periods with $B_y < 0$ without a significant difference between the fluxes measured above the weak and strong sources at $h \geq 600 \text{ km}$. At lower altitudes attenuation of fluxes is observed even for moderate B_{cr} ($\sim 50\text{--}70 \text{ nT}$).

Asymmetry of electron fluxes is not very sensitive to a sign of the vertical/ horizontal component of the crustal magnetic field (Fig. 7) that may imply a rather complicated reconnection pattern.

Only rare spikes of the electron fluxes with values $> 10^9 \text{ cm}^{-2} \text{ s}^{-1}$ are observed at the altitudes less than 400 km . An abrupt drop of electron fluxes at $h \sim 600 \text{ km}$ can seriously constrain models of electron precipitation into the nightside atmosphere and aurora on Mars although without information about their pitch-angle distribution such a conclusion must be treated as tentative.

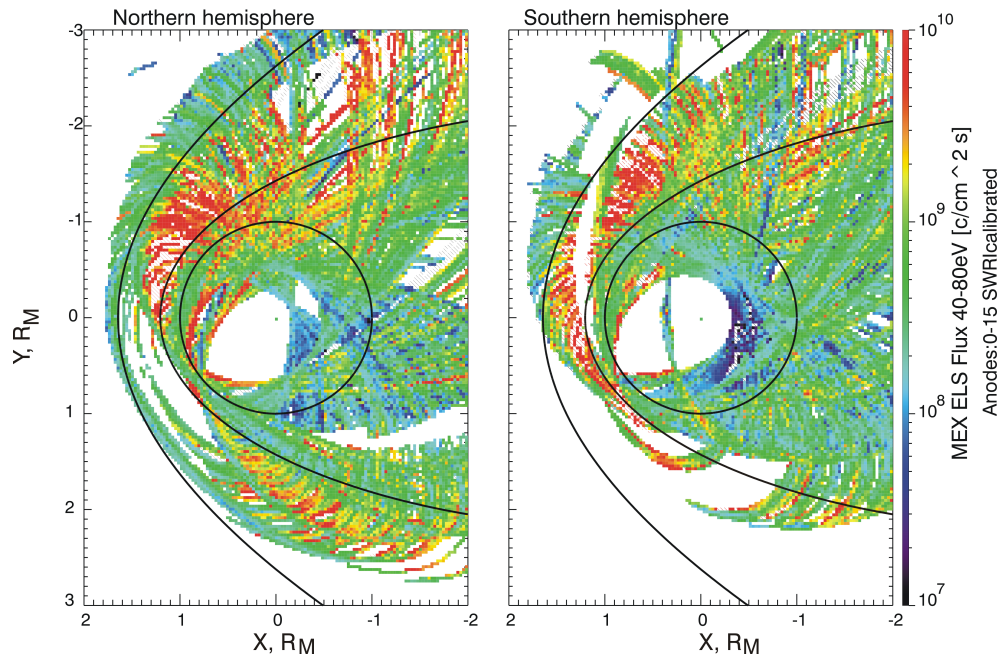


Fig. 10. Map of median electron fluxes ($40\text{ eV} < E < 80\text{ eV}$) in the XY (MSO) noon-midnight planes for the Southern and Northern Hemispheres.

It is worth noting that in the Northern Hemisphere, where crustal fields are much weaker and reconnection processes do not operate, an asymmetry related to the sign of $B_{y\text{IMF}}$ is not seen (Fig. 8).

3.3 Global maps of electron fluxes

It is interesting to compare the fluxes of electrons penetrating to low altitudes with typical fluxes in the magnetosheath and within the Martian magnetosphere. Figure 9 presents a map of electron fluxes ($40\text{ eV} < E_e < 80\text{ eV}$) in the XZ (MSO) noon-midnight plane. To increase the sampling coverage we use all measurements made at radial distances r closer than $2.5 R_M$, where $r = (Y^2 + Z^2)^{1/2}$ is the radial distance in cylindrical coordinates. This explains the appearance of bow-shaped structures inside the magnetosphere. Median fluxes in the magnetosheath often exceed values of $\sim 10^{10}\text{ cm}^{-2}\text{ s}^{-1}$. Maximum values reach $5 \times 10^{11}\text{ cm}^{-2}\text{ s}^{-1}$. The region of strong crustal magnetic field shielding an access of solar wind electrons in the Southern Hemisphere at the nightside is clearly seen (a blue spot). The height of the shielding screen is about 500 km. Fluxes with intensity of $10^8 - 10^9\text{ cm}^{-2}\text{ s}^{-1}$ correspond to the lobe regions. For active periods fluxes in the lobe can easily reach $10^{10}\text{ cm}^{-2}\text{ s}^{-1}$.

An effect of crustal sources can be better observed if we use only the measurements carried out in the planetocentric longitude range of $130^\circ - 240^\circ$ which corresponds to the strongest magnetizations. Figure 10 shows maps of electron fluxes in the central XY (MSO)-plane. The data from the measurements made at $r < 2 R_M$, $130^\circ < \text{Long} < 240^\circ$ were

projected onto the XY plane separately for the observations in the Northern and Southern Hemispheres. Comparison of these two maps clearly shows the effect of the magnetic field screening not only at the nightside but also in the day and dawn sectors. There is also a dawn-dusk asymmetry of electron fluxes at $X < 0$. Its origin is probably associated with a draping asymmetry arising due to the X-component of the IMF. For the Parker IMF orientation the field lines at the dawn side have a normal component at the magnetospheric boundary and the sheath electrons have a more easy access into the magnetosphere. The observations on MGS by Bertucci et al. (2005) have shown that there is a normal while a small component of the magnetic field at the magnetospheric boundary. This asymmetry is observed in both hemispheres (see also Dubinin et al., 2008a).

3.4 Electron precipitation and aurora on Mars

Bertaux et al. (2005) have observed very localized CO Cameron band emissions produced by electron impact dissociation of CO_2 molecules and CO_2^+ emissions produced by ionization of CO_2 molecules which were clearly associated with the existence of strong crustal fields. The ratio of their intensities set a strong constraint on the energies of the parent electrons (Leblanc et al., 2006). The best agreement with the optical observations is obtained for energy distributions peaking at energies below a few tens of eV. Narrow spikes of suprathermal electrons with such energies were observed on the night-side of Mars by ASPERA-3 (Dubinin et al., 2008b). Dubinin et al. (2008b) suggested that electron

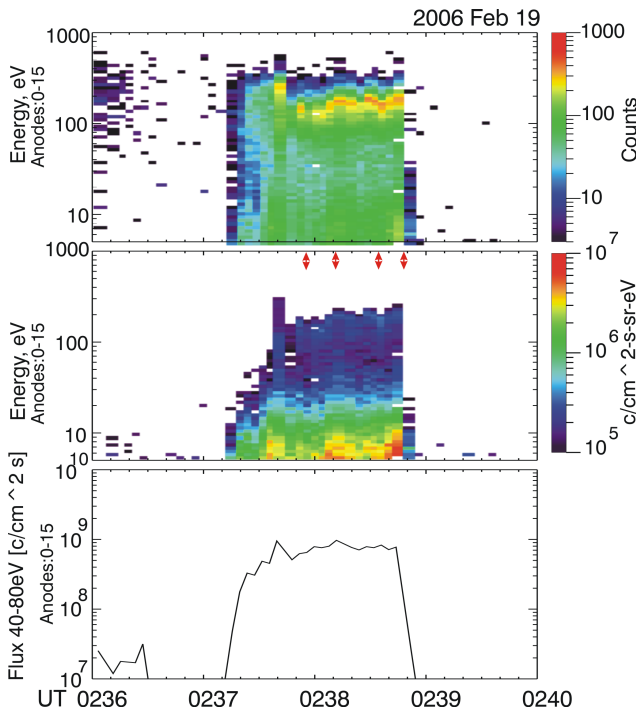


Fig. 11. Spectrogram of electron fluxes measured by ELS-ASPERA-3 during the UV observations of aurora and total fluxes of electrons ($40 \text{ eV} < E < 80 \text{ eV}$). The top (middle) panel shows spectra as a function of $C(E)$ ($j(E)$), respectively. The peaks in $C(E)$ visible above 100 eV are almost vanish when plotting differential flux $j(E)$.

fluxes of $2 \times 10^6 \text{ cm}^{-2} \text{ s}^{-1} \text{ ster}^{-1} \text{ eV}^{-1}$ (that approximately corresponds to $F = 4\pi j \Delta E \sim 10^9 \text{ cm}^{-2} \text{ s}^{-1}$) in such events could explain the observed auroral UV emissions (Bertaux et al., 2005; Leblanc et al., 2006).

Figure 11 shows the spectrogram of electron fluxes and the total flux F in the energy range $40\text{--}80 \text{ eV}$ from the ASPERA-3 observations when the UV spectrometer SPICAM measured the aurora-type emissions in the nadir direction (Leblanc et al., 2008). Intervals during which the aurora emissions were identified are also shown. Observations were made at rather low altitudes ($300\text{--}350 \text{ km}$) above the strong crustal sources. It is observed that during these events fluxes of suprathermal electrons exceed $10^9 \text{ cm}^{-2} \text{ s}^{-1}$.

Electrons which penetrate to altitudes $h \leq 400 \text{ km}$ in the regions of strong crustal fields form a spatially well organized pattern with bands stretched in the longitudinal direction (see also Brain, 2006c). Figure 12 shows maps of electron fluxes in the energy range $30\text{--}80 \text{ eV}$ and $100\text{--}300 \text{ eV}$ measured on the MGS spacecraft by the MAG/ER instrument at $h \sim 400 \text{ km}$ in the night sector ($\sim 02:00 \text{ LT}$). The data are shown in the planetocentric eastern longitude and latitude coordinates for the longitude range $160^\circ\text{--}240^\circ$ of the Southern Hemisphere where the strongest crustal sources of the magnetic field are located. The patterns

Table 1. Dates and times of aurora events.

	Date	Time	Alt, km
1	7 Jul 2004	05:39:52–05:39:55	670
2	7 Jul 2004	05:41:17–05:41:36	586
3	26 Jan 2006	14:04:01–14:04:15	564
4	19 Feb 2006	02:37:56–02:38:11	387
5	19 Feb 2006	02:38:34–02:38:48	365
6	19 Feb 2006	02:40:52–02:41:02	309
7	27 Dec 2005	21:47:31–21:47:41	954
8	27 Dec 2005	21:51:08–21:51:16	700

are similar for positive and negative $B_{y\text{IMF}}$ although a certain asymmetry with higher fluxes at $B_{y\text{IMF}} < 0$ still exists. The ordering of the precipitating electrons is guided by the crustal field shown in Fig. 12d. Median values of fluxes vary in the range of $10^7\text{--}2 \times 10^8 \text{ cm}^{-2} \text{ s}^{-1}$ ($30\text{--}80 \text{ eV}$) and $5 \times 10^6\text{--}3 \times 10^7 \text{ cm}^{-2} \text{ s}^{-1}$ ($100\text{--}300 \text{ eV}$). The bands of increased “precipitation” are observed in most regions with strong vertical component of the crustal field (Fig. 12d). Generally, median electron fluxes in the precipitation pattern have values less than $10^9 \text{ cm}^{-2} \text{ s}^{-1}$ and therefore aurora emissions can be observed only at the periods of enhanced precipitation. This is in agreement with the observations made by Leblanc et al. (2008) who have measured only 8 events on 21 orbits above the regions with strong crustal sources.

Maximum values of electron fluxes in the precipitation bands shown in Fig. 13a can explain the SPICAM observations of auroral-type emissions. Crosses in Fig. 13a depict positions of aurora events identified in the SPICAM UVS data (Leblanc et al., 2008). Numbers correspond to orbits given in the table adopted from Leblanc et al. (2008). Figure 13c presents fluxes of electrons recorded by the ASPERA-3 at altitudes of $250\text{--}600 \text{ km}$ for the same time period. The measurements were made closer to the terminator at solar zenith angles $< 130^\circ$. Due to a difference in the spacecraft orbits (the orbit of MEX is elliptical, the orbit of MGS is circular) the data coverage of the MEX observations is less than that of MGS. Nevertheless ASPERA-3 also detects longitudinally stretched narrow precipitation bands which could be a site of aurora on Mars.

3.5 Peaked electron distributions (inverted “V” structures)

Peaked electron distributions on Mars were observed at different altitudes on MGS and MEX (Brain et al., 2006a; Lundin et al., 2006). Analogy with inverted V structures in the Earth magnetosphere raised the questions whether aurora on Mars exist and whether there are significant field-aligned electric potential drops on the crustal field lines. Although much higher values of the Pedersen conductivity of the Martian ionosphere, as compared to the Earth case, set strong constraints on the value of the field-aligned potential drops

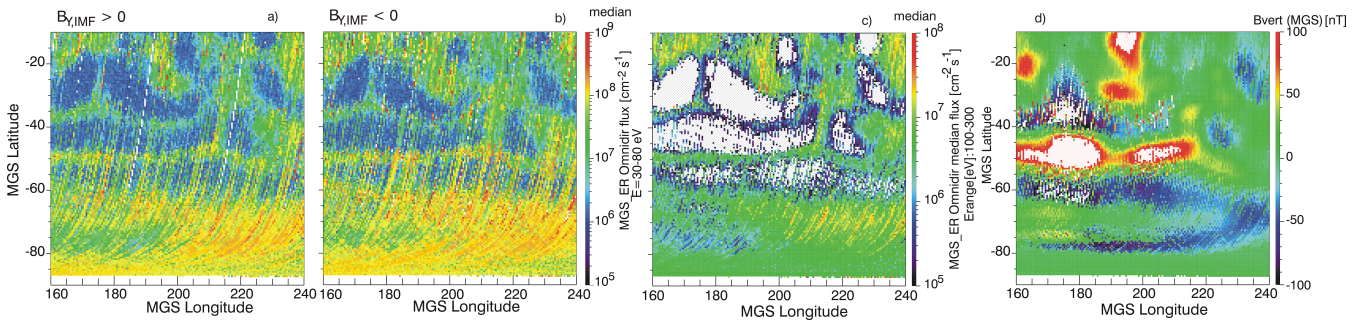


Fig. 12. (a, b) Precipitation patterns of median fluxes of the electrons with $30 < E_e < 80$ eV measured on the MGS at $h \sim 400$ km at the positive and negative B_{yIMF} . (c) precipitation pattern of electrons with $100 < E_e < 300$ eV, (d) vertical component of the crustal magnetic field.

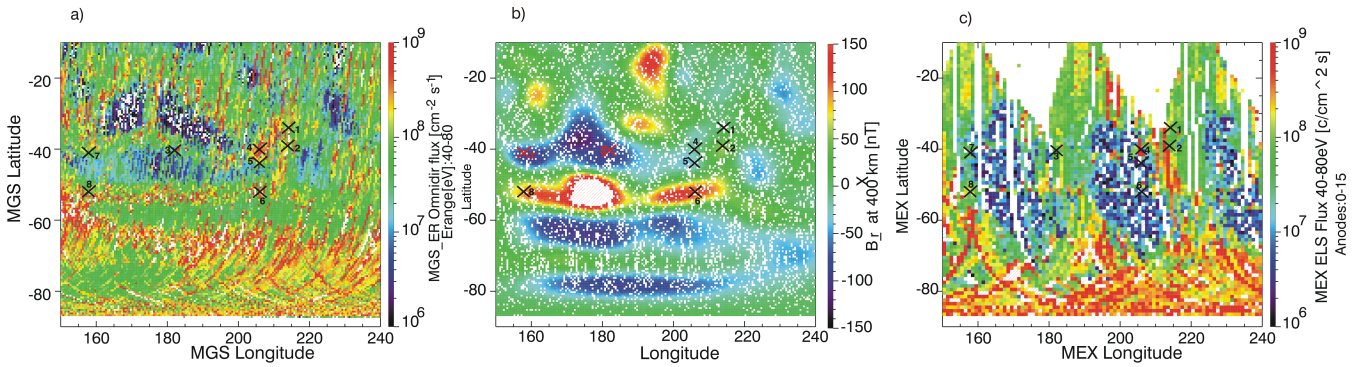


Fig. 13. (a) Precipitation patterns of maximum fluxes of the electrons with $30 < E_e < 80$ eV measured on MGS at $h \sim 400$ km, (b) vertical component of the crustal magnetic field, (c) precipitation pattern of the electrons with $40 < E_e < 80$ eV measured on the MEX spacecraft at $250 \leq h \leq 600$ km. Positions of aurora events observed by SPICAM viewing in the nadir are shown by crosses.

and the width of “auroral” structures (Dubinin et al., 2008c) such configurations are possible.

We have analyzed about 1500 events during two years of the MEX operation with peaks on differential flux spectra which could be candidates for aurora on Mars. Note that maxima on spectra often appear while plotting $C(E)$ (C is a count rate or differential energy flux, E is electron energy) but also often vanish if differential fluxes $J(E)$ are plotted ($J \sim C/E$) (see e.g. Fig. 11). Figure 14 (the top panels) presents a spatial distribution of all events in the XZ and YZ (MSO) coordinates. Color on the left and middle panels shows the peak electron energy inferred from the differential spectra of electron fluxes. Color on the right panels shows the value of the differential flux corresponding to the peak energy. Events are observed in both hemispheres (not only in the southern one where crustal sources are localized) and at different distances from the planet. The maximum peak energies are measured at a large distance from Mars. There is also no clear trend of a peak energy increase with decreasing altitude as would be expected if we exploit a simple analogy with auroral processes on the Earth. On the other hand, fluxes are stronger in the Southern Hemisphere, closer to the planet. It worth noting that in aurora on Earth both

values, namely, the number flux of electrons and parallel potential voltage which can be inferred from the peaks in the energy spectra are equally responsible for the energy deposition in the atmosphere. The bottom panels show spatial distributions of the “inverted V” events in the coordinates determined by the IMF orientation (this system has the X^* -axis antiparallel with the upstream solar wind flow, the Y^* -axis along the cross-flow magnetic field component of the IMF, and the Z^* -axis along the direction of the motional electric field $E = -\mathbf{V} \times \mathbf{B}_{IMF}$, where \mathbf{B}_{IMF}). Recall here that the magnetic field \mathbf{B}_{IMF} is only a proxy from the MGS measurements on its circular orbit at 400 km since there is no magnetometer on MEX. Almost all peaked distributions are observed in the hemisphere into which the motional electric field is pointing. A map of planetary ion beams (not shown here), which often accompany the electron events with a peaked distribution, is similar.

Since heavy planetary ions (O^+ , O_2^+ , CO_2^+) moving in the electric field driven by solar wind are not magnetized, ion and electron trajectories do not coincide. This can lead to the appearance of positive potential spikes and, correspondingly, to field-aligned fluxes of sheath electrons to supply a quasi-neutrality and provide $\text{div} \mathbf{j} = 0$, where \mathbf{j} is the current density.

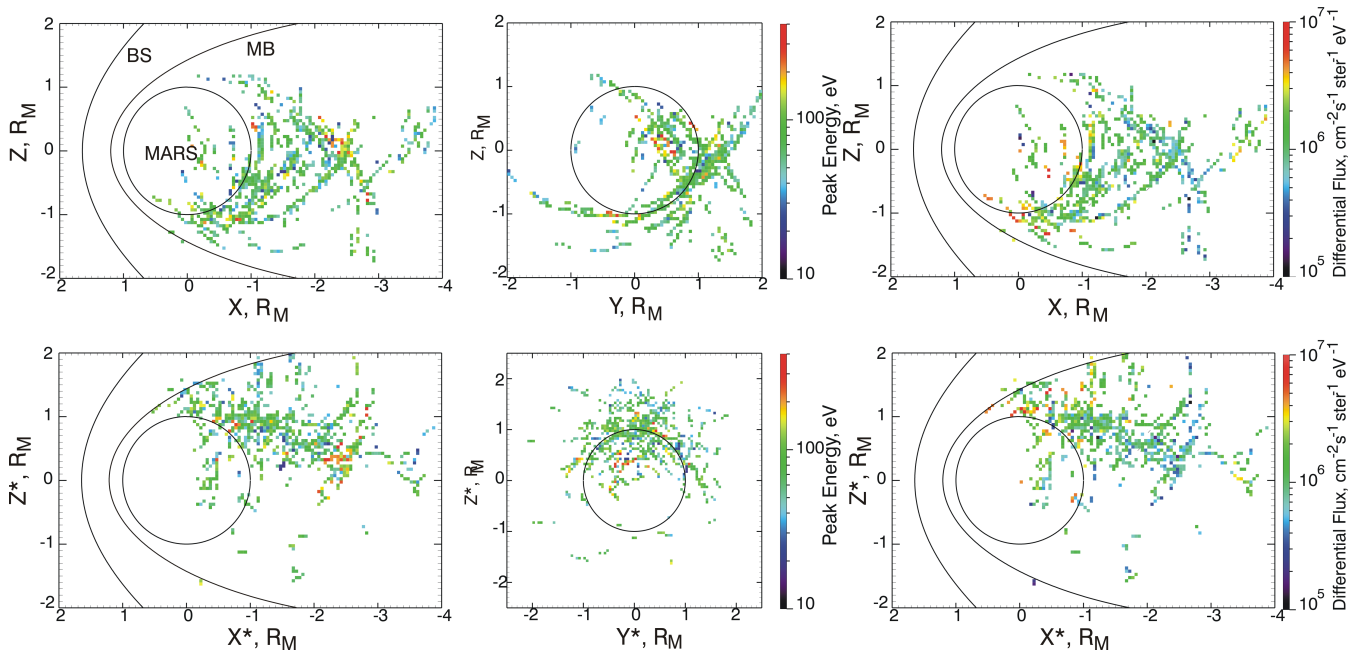


Fig. 14. (top) Maps of the events with peaked electron spectra in MSO coordinates, (bottom) maps in the coordinate system determined by the IMF direction. Color shows the peak energy of electrons (left and middle panels) and the differential flux corresponding to the peak energies (right panels).

Conservation of the electron magnetic moment in the piled up region of the Martian magnetosphere where the magnetic field strength increases results in a more isotropic distribution of the peaked electrons. Hence, in the relationship between ion beams and peaked electrons, ions is the cause and peaked electrons is the effect.

It is worth noting that peaked electron distributions on the auroral force tubes at Earth arise due to different angular distributions of ions and electrons in the geomagnetic field, i.e. they are also the result of a coherent action of a combination of electrostatic potential and mirror-like magnetic field configuration. A similar combination is met at the bow shock where solar wind electrons stream to mirror-like field with a positive potential and explains the appearance of top-flat electron distributions. Note here, that the peaked electron spectra on Mars plotted as f versus E , where f is the distribution function ($f \sim J/E$) mostly occur as monotonically decreasing functions of energy with a shoulder-top flat distributions.

Resuming, peaked electron spectra may appear in various plasma configurations with similar physical processes operating. For the discussed class of events the mechanism associated with the spikes of extracted planetary ions seems to be preferable. Such a mechanism generally explains many observational facts, namely, absence of an altitude dependence in the peak electron energy, a clustering of the events in the hemisphere into which the motional electric field is pointing (planetary ions dominate in this hemisphere) and the obser-

vations of such structures in the Northern Hemisphere where a role of the crustal field is not important.

Other mechanisms which were mentioned above can also contribute to the appearance of the peaked electron distributions on Mars. Brain et al. (2006a) have observed a clear relationship between the occurrence of peaked electron distributions at the altitude of ~ 400 km and the crustal fields. They have also shown that the IMF orientation strongly affects whether these electrons are observed. Peaked distributions were preferentially measured at $B_{y\text{IMF}} < 0$ which is in an agreement with a preferential access of solar wind electrons to the Southern Hemisphere when the motional electric field is pointed southward. Top-flat distributions at the bow shock can also give rise to similar characteristics inside the magnetosphere when magnetosheath electrons penetrate inward along the draped magnetic field lines. A plasma injection in thin current sheets in the reconnection processes is another source of such type distributions.

4 Conclusions

We have explored the access of the magnetosheath electrons ($40 \leq E_e \leq 80$ eV) into the Martian magnetosphere, and the role of the IMF and crustal magnetic fields. It is shown that crustal sources in the Southern Hemisphere located in the longitude range of 130° – 240° contribute essentially to the pressure of the obstacle deflecting solar wind around Mars on the dayside. The magnetospheric boundary moves upward

by $\sim 400\text{--}500$ km. Asymmetry in an obstacle shape creates an asymmetry in the position of the bow shock. Superposition of contributions from different local crustal sources provides approximately a linear altitude dependence of an “access boundary” with the field strength. The position of the magnetospheric boundary weakly depends on the sign of the cross-flow component of the IMF. On the other hand, the Parker IMF configuration influences access of the electrons on the dawn and dusk side. Due to the appearance of a normal component of the draped magnetic field the magnetosheath electrons penetrate deeper in the dawn sector. A precipitation pattern at altitudes ≤ 400 km in the crustal field area is well regulated by the field distribution. Electrons mainly occupy the regions with a weak vertical component of the magnetic field with some clear signatures of cusp-like intrusions.

On the nightside, crustal sources also create a protection screen significantly reducing electron fluxes below ~ 600 km. Only rare spikes of the median electron fluxes with values $> 10^9 \text{ cm}^{-2} \text{ s}^{-1}$ are observed at altitudes less than 400 km. Such fluxes of suprathermal electrons are necessary to explain the aurora observed by SPICAM on the nightside of Mars. Access of electrons at $h \geq 600$ km is strongly controlled by the IMF orientation. The negative sign of $B_{y\text{IMF}}$ increases the probability of high electron fluxes above the regions with strong crustal sources. A more easy access of electrons is probably caused by reconnection between the draped magnetic field of solar wind origin and crustal fields.

Electron precipitation on the nightside consists of intermittent longitudinally stretched narrow bands which follow the bands with a strong vertical component of the field. Maximum values of fluxes measured in such bands can easily produce aurora and increased ionization.

On the other hand, the occurrence of another class of electron distributions resembling inverted “V” structures typical for the auroral field tubes on Earth, is controlled by external factors – as IMF orientation. Almost all such structures are observed in the hemisphere into which the motional electric field is pointing. There is also no visible trend of a peak energy increase with decreasing altitude. The mechanism of the formation of these structure is probably a result of a coherent action of macroscopic positive potential jumps and field-aligned electron flows in mirror magnetic field configurations to supply quasi-neutrality.

Acknowledgements. E. D. thanks the Deutsche Forschungsgemeinschaft and the Max-Planck-Gesellschaft for supporting this work by grant (WO 910/1-P). E. D., M. F. and J. W. also thank the DLR support by grants 50QM99035 and FKZ 50 QM 0801. We thank the MAG-ER team and the UCLA PPI node for making the MGS magnetic field electron data available.

Topical Editor I. A. Daglis thanks P. Israelevich and C. Mazelle for their help in evaluating this paper.

References

- Acuña, M. H., Connerney, J. E. P., Wasilewski, P., et al.: The Mars Observer Magnetic Fields Investigation, *J. Geophys. Res.*, 97, 7799–7814, 1992.
- Acuña, M. H., Connerney, J., Wasilewski, P., et al.: Magnetic field and plasma observations at Mars: initial results of the Mars Global Surveyor MAG/ER experiment, *Science*, 279, 790–793, 1998.
- Barabash, S., Lundin, R., Andersson, H., et al.: The analyzer of space plasma and energetic atoms (ASPERA-3) for the Mars Express mission, *Space Sci. Rev.*, 126, 113, doi:10.1007/s112-006-9124-8, 2006.
- Bertaux, J.-L., Leblanc, F., Witasse, O., et al.: Discovery of an aurora on Mars, *Nature*, 435, 790–794, doi:10.1038/nature03603, 2005.
- Bertucci, C., Mazelle, C., Crider, D., et al.: Magnetic field draping enhancement at the Martian magnetic pileup boundary from MGS observations, *Geophys. Res. Lett.*, 30(2), 1099, doi:10.1029/2002GL015713, 2003.
- Bertucci, C., Mazelle, C., Acuña, M. H., Russell, C. T., and Slavin, J. A.: Structure of the magnetic pileup boundary at Mars and Venus, *J. Geophys. Res.*, 110, A01209, doi:10.1029/2004JA010592, 2005.
- Böswetter, A., Bagdonat, T., Motschmann, U., and Sauer, K.: Plasma boundaries at Mars: A 3-D simulation study, *Ann. Geophys.*, 22, 4363–4379, 2004, <http://www.ann-geophys.net/22/4363/2004/>.
- Brain, D. A., Halekas, J. S., Peticolas, L. M., Lin, R. P., et al.: On the origin of aurora on Mars, *Geophys. Res. Lett.*, 33, L01201, doi:10.1029/2005GL024782, 2006a.
- Brain, D. A., Mitchell, D. L., and Halekas, J. S.: The magnetic field draping direction at Mars from April 1999 through August 2004, *Icarus*, 182, 464, doi:10.1016/j.icarus.2005.09.023, 2006b.
- Brain, D. A.: Mars Global Surveyor measurements of the Martian solar wind interaction, *Space Sci. Rev.*, 126, 77, doi:10.1007/s11214-006-9122-x, 2006c.
- Brain, D. A., Lillis, R. J., Mitchell, D. L., et al.: Electron pitch-angle distributions as indicators of magnetic field topology near Mars, *J. Geophys. Res.*, 112, A09201, doi:10.1029/2007JA012435, 2007.
- Cain, J. C., Ferguson, B., and Mozzoni, D.: An $n=90$ internal potential function of the Martian crustal field, *J. Geophys. Res.*, 108(E2), 5008, doi:10.1029/2000JE001487, 2003.
- Connerney, L. E., Acuña, M., Wasilewski, P., Kletetschka, G., Ness, N. F., Reme, H., Lin, R., and Mitchell, D.: The global magnetic field of Mars and implications for crustal evolution, *Geophys. Res. Lett.*, 28, 4015–4018, 2001.
- Crider, D. H., Acuña, M., Connerney, J. E. P., et al.: Observations of the latitude dependence of the location of the Martian magnetic pileup boundary, *Geophys. Res. Lett.*, 29(8), 1170, doi:10.1029/2001GL013860, 2002.
- Dubinin, E., Lundin, R., and Schwingschuh, K.: Solar wind electrons as tracers of the Martian magnetotail topology, *J. Geophys. Res.*, 98, 21 233–21 240, 1994.
- Dubinin, E., Fraenz, M., Woch, J., et al.: Plasma morphology at Mars. ASPERA-3 observations, *Space Sci. Rev.*, 126, 209, doi:10.1007/s11214-006-9039-4, 2006.
- Dubinin, E., Fraenz, M., Woch, J., et al.: Suprathermal electron fluxes on the nightside of Mars. ASPERA-3 observations, *Planet.*

- Space Sci., 56, 846, doi:10.1016/j.pss.2007.12.010, 2008a.
- Dubinin, E., Chanteur, G., Fraenz, M., et al.: Asymmetry of plasma fluxes at Mars. ASPERA-3 observations and hybrid simulations, *Planet. Space Sci.*, 56, 832, doi:10.1016/j.pss.2007.12.006, 2008b.
- Dubinin E., Chanteur, G., Fraenz, M., and Woch, J.: Field-aligned currents and parallel electric field potential drops at Mars. Scaling from the Earth' aurora, *Planet. Space Sci.*, 56, 868, doi:10.1016/j.pss.2007.01.019, 2008c.
- Fedorov, A., Budnik, E., Savaud, J.-A., et al.: Structure of the martian wake, *Icarus*, 182, 320, doi:10.1016/j.icarus.2005.09.021, 2006.
- Fraenz, M., Winningham, J. D., Dubinin, E., Roussos, E., et al.: Plasma intrusion above Mars crustal fields-Mars Express ASPERA-3 observations, *Icarus*, 182, 406, doi:10.1016/j.icarus.2005.11.016, 2006.
- Frahm, R., Winningham, J. D., Sharber, J. R., et al.: Carbon dioxide photoelectron energy peaks at Mars, *Icarus*, 182, 371, doi:10.1016/j.icarus.2006.01.014, 2006.
- Leblanc, F., Witasse, O., Winningham, J., et al.: Origin of the martian aurora observed by spectroscopy for investigation of characteristics of the atmosphere of Mars (SPICAM) onboard Mars Express, *J. Geophys. Res.*, 111, A09313, doi:10.1029/2006JA011763, 2006.
- Leblanc, F., Witasse, O., Liliensten, J., et al.: Observations of aurores by SPICAM ultraviolet spectrograph on board Mars Express: Simultaneous ASPERA-3 and MARSIS measurements, *J. Geophys. Res.*, 113, A08311, doi:10.1029/2008JA013033, 2008.
- Lundin, R., Winningham, J. D., Barabash, S., et al.: Plasma acceleration above Martian magnetic anomalies, *Science*, 311, 980, doi:10.1126/science.1122071, 2006.
- Mitchell, D. L., Lin, R. P., Mazelle, C., et al.: Probing Mars' crustal magnetic field and ionosphere with the MGS electron reflectometer, *J. Geophys. Res.*, 106, 23 419–23 427, 2001.
- Mitchell, D. L., Lillis, R. J., Lin, R. P., et al.: A global map of Mars' crustal magnetic field based on electron reflectometry, *J. Geophys. Res.*, 112, E1002, doi:10.1029/2005JE002564, 2007.
- Modolo, R., Chanteur, G., Dubinin, E., and Matthews, A.: Influence of the solar activity on the Martian plasma environment, *Ann. Geophys.*, 23, 433–444, 2005, <http://www.ann-geophys.net/23/433/2005/>.
- Nagy, A. F., Winterhalter, D., Sauer, K., et al.: The plasma environment on Mars, *Space Sci. Rev.*, 111, 33, doi:10.1023/B:SPAC.0000032718.47512.92, 2004, 2005.
- Roussos, E., Fraenz, M., Dubinin, E., et al.: Energetic electron asymmetries in the Martian magnetosphere. ASPERA-3 observations, *Planet. Space Sci.*, 56, 836, doi:10.1016/j.pss.2007.12.009, 2008.
- Soobiah, Y., Coates, A., Linder, D., et al.: Observations of magnetic anomaly signatures in Mars Express ASPERA-3 ELS data, *Icarus*, 182, 396, doi:10.1016/j.icarus.2005.10.034, 2006.
- Trotignon, J.-G., Mazelle, C., Berucci, C., and Acuña, M. H.: Martian shock and magnetic pile-up boundary position and shapes determined from the Phobos 2 and Mars Global Surveyor data sets, *Planet. Space Sci.*, 54, 357, P11A-0968, 2006.
- Vennerstrom, S., Olsen, N., Purucker, M., and Acuña, M.: The magnetic field in the pile-up region at Mars, and its variations with the solar wind, *Geophys. Res. Lett.*, 30, 1369, doi:10.1029/2003GL016883, 2003.
- Vignes, D., Mazelle, C., Reme, H., Acuña, M., et al.: The solar wind interaction with Mars: Locations and shapes of the bow shock and magnetic pile-up boundary from the observations of the MAG/ER experiment onboard Mars Global Surveyor, *Geophys. Res. Lett.*, 27, 49–52, 2000.
- Vignes, D., Acuña, M., Connerney, J. E. P., et al.: Factors controlling the location of bow shock At Mars, *Geophys. Res. Lett.*, 29(9), 1328, doi:1029/2001GL014513, 2002.
- Winningham, J. D., Frahm, R. A., Sharber, J. R., et al.: Electron oscillations in the induced Martian magnetosphere, *Icarus*, 182, 360, doi:10.1016/j.icarus.2005.10.033, 2006.